Metrol. Meas. Syst., Vol. 33 (2026) No. 1, pp. 1–16
DOI: 10.24425/mms.2026.158367

PAN POLSKA AKADEMIA NAUK

METROLOGY AND MEASUREMENT SYSTEMS

Index 330930, ISSN 0860-8229
www.metrology.wat.edu.pl

M&MS

IMPROVED POINTNET-BASED BINOCULAR STRUCTURED LIGHT DETECTION FOR CERAMIC BALL DEFECTS

Gang Cheng[1)], Xu-Yi Miao[1)], Guo-Qing Gu[2)], Jing-Yi Yan[3)], Jian-Zhou Du[4)]

1) School of Mechanical Engineering, Yancheng Institute of Technology, Yancheng 224051, China
2) School of Civil Engineering, Yancheng Institute of Technology, Yancheng 224051, China (*gqgu@ycit.edu.cn*)
3) Jiangsu Dongpu Fine Ceramic Technology Co. Ltd, Lianyungang 222000, China
4) School of Materials Science and Engineering, Yancheng Institute of Technology, Yancheng 224051, China

Abstract

To address low accuracy in defect detection of point clouds from binocular structured light 3D reconstruction caused by high reflectivity of the surface of silicon nitride ceramic balls, this study proposes a method integrating PointNetLK point cloud registration and PointNet++ defect recognition networks. Initially, PointNet segments and removes reflective regions from the point clouds. Subsequently, an enhanced PointNetLK network performs high-precision binocular point cloud registration with missing region compensation, demonstrating two orders of magnitude improvement in registration accuracy over the conventional Coherent Point Drift (CPD) + Iterative Closest Point (ICP) methods. Finally, the compensated complete point clouds are processed by an enhanced PointNet++ network incorporating a Multi-Scale Grouping (MSG) strategy for defect segmentation, effectively identifying two primary defect types (pits and scratches) with an average mIoU of 0.8565. Ablation studies confirm the critical contributions of the Set Abstraction (SA) module and MSG strategy. This approach significantly mitigates hyper-reflection interference, achieving high-precision, robust, and non-destructive quantification of ceramic ball surface defects.

Keywords: ceramic balls, defects detection, binocular structured light, point cloud reconstruction, PointNet.

1. Introduction

Silicon nitride ceramics, characterised by their lightweight nature, high hardness, exceptional strength, low friction coefficient, excellent thermal resistance, electrical insulation properties, and extraordinarily long service life, have been widely applied in the bearing systems of drive motors for new energy vehicles [1–3]. Due to the inherent brittleness of ceramic materials, coupled with complex manufacturing processes and sensitive process parameters, sporadic surface defects frequently occur on ceramic balls. Since surface quality directly impacts both bearing performance and the operational life of entire systems [4], such imperfections not only substantially compromise

Article history: received 26, 2025; revised December 9, 2025; accepted January 23, 2026; available online March 13, 2026.

the mechanical integrity of ceramic balls but also can trigger premature fatigue failure, severely jeopardising system reliability and stability [5]. Consequently, implementing high-precision non-destructive inspection of finished ceramic balls is urgently required to effectively mitigate performance degradation caused by surface defects.

Currently, traditional surface defect detection methods for ceramic balls include mainly manual visual inspection, radiographic testing, ultrasonic flaw detection, computed tomography (CT) technology, etc. [6]. For example, Deneuville *et al.* [7] have initially proposed an ultrasonic detection system specifically for ceramic balls of silicon nitride, but the device requires that the diameter of the ceramic ball to be tested be not less than 50 mm, which has significant limitations in practical production. It turned out, however, that industrial CT technology has high detection accuracy and can achieve high-precision detection of structural components, making further inspection of ceramic balls possible. Chlebus *et al.* [8] applied CT detection to additive manufacturing of composite materials, using 3D modelling to analyse the unmelted metals rhenium and molybdenum in 3D printing, in order to analyse the strength of the parts. However, the high cost and huge volume of CT equipment limit its widespread application in general industrial fields. Lei *et al.* [9] introduced an error compensated CNN model that analyses variations in ultrasonic signals to locate flow-induced void defects within ceramic materials, showing promising potential for industrial applications. In addition, Zhang *et al.* [10] proposed a method for surface defect detection based on fringe reflection technology. If a ceramic ball is non-defective, the image, formed by reflection on its surface, presents even fringes. The distortion of fringes designed by a reverse exact ray-tracing method occurs at the defective region of ceramic balls.

In recent years, with the help of computer vision, industrial cameras, and image processing technology, machine vision systems have been able to achieve millimetre or even micrometre level surface defect detection, becoming an important development direction for intelligent detection of defects in ceramic balls [11]. In the quality inspection of ceramic balls, deep learning technology is gradually replacing traditional manual feature engineering and rule matching methods, becoming one of the main detection methods. For example, Xu *et al.* [12] proposed an improved YOLO11-based defect detection method tailored for ceramic bearing balls to address the limitations of conventional image-processing methods in detecting intricate and variable surface defects. Li *et al.* [13] submitted a multi-view surface defect detection of ceramic bearing balls integrating features enhanced by the *Gabor salient domain* (GSMF). By improving the co-attention of the multi-view to prevent memory loss caused by long-distance transmission, more feature information of the ceramic balls was preserved effectively. Jiang *et al.* [14] studied a detection method for surface defects in ceramic bearing balls based on a cartoon texture decomposition model to improve the detection accuracy. Similarly, Yu *et al.* [15] proposed a defect detection algorithm based on the *stationary wavelet transform* (SWT) and nonlinear enhancement to improve the detection accuracy and efficiency of silicon nitride ceramic ball surface defects. However, the results of the above research still have not effectively solved the crucial problem of low machine learning detection accuracy caused by the high reflectivity on the surface of ceramic balls. Due to the fact that surface defects on ceramic balls can be to some extent located in a highly reflective region, it is quite difficult to guarantee the accuracy of machine vision-based detection methods.

To address this, this paper innovatively proposes a binocular structured light point cloud detection method for ceramic ball defects that integrates the PointNetLK and PointNet++ network architectures. By enabling precise segmentation of reflective regions, achieving high-accuracy registration and missing data compensation for binocular point clouds, and incorporating multi-scale feature extraction with localised perception mechanisms, the proposed method realises refined detection of surface defects on ceramic balls, significantly enhancing the robustness and accuracy of defect identification.

2. Binocular Structured Light 3D Measurement for Ceramic Balls

2.1. Common Defects of Ceramic Balls

Surface defects on silicon nitride ceramic balls primarily fall into four categories: pores, pits, erosions, and scratches, as illustrated in Fig. 1. Among these, pits and scratches occur most frequently in all processing stages of ceramic ball production, constituting defects of structural integrity. These two types of defects not only degrade the smoothness of the surface through wear but also act as initiation sites for crack propagation. In addition, they severely interfere with optical inspection processes, substantially compromising the accuracy of defect recognition. Consequently, this study specifically focuses on developing high-precision non-destructive testing methods tailored to detect pit and scratch defects.

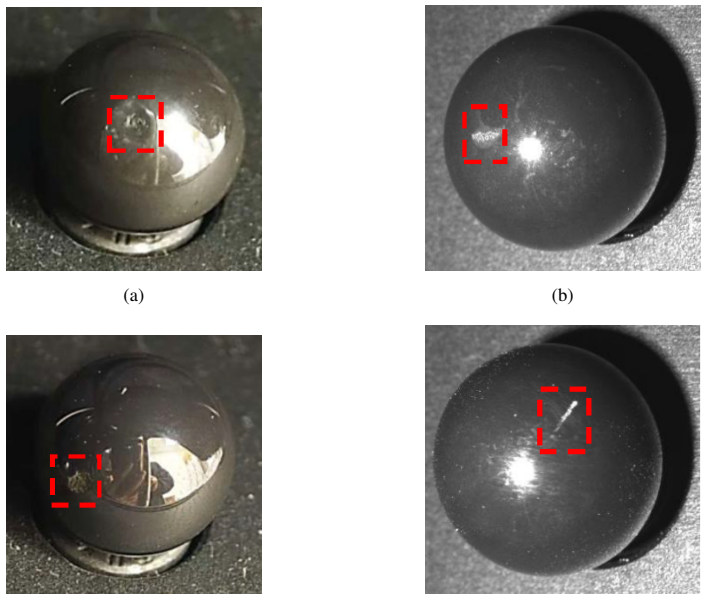

Fig. 1. Surface defects of silicon nitride ceramic balls: a) pore, b) pit, c) erosion, and d) scratch.

2.2. Reconstruction of Binocular Structured Light Point Cloud

Figure 2 illustrates a schematic diagram of a 3D binocular structured light measurement system for ceramic balls. Firstly, a structured light encoding pattern is projected onto the surface of a ceramic ball by a projector. This pattern is modulated by the surface morphology of the ceramic balls and contains their three-dimensional information. Subsequently, the dual-camera captures the modulated pattern and processes it through the corresponding decoding algorithms to accurately calculate the spatial information on the surface points of the ceramic ball. Finally, by combining structural light decoding and encoding algorithms such as binocular calibration [16], phase unwrapping [17], and stereo vision matching [18], a 3D reconstruction of the surface morphology of ceramic balls can be achieved.

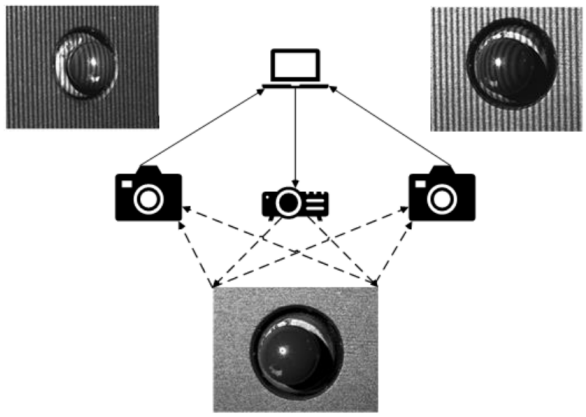

Fig. 2. Schematic diagram of the binocular structured light system.

Figure 3 shows the reconstructed contour point cloud of the surface of the ceramic ball. It is not difficult to observe that the highly reflective areas on the surface of ceramic balls can lead to a certain degree of loss in the three-dimensional reconstructed point cloud data obtained from epipolar correction. Therefore, it is necessary to use point cloud post-processing technology to achieve complete and accurate reconstruction of ceramic ball point clouds, accurately locate and eliminate highly reflective areas, and then use the compensated complete point cloud for subsequent detection to minimise reflective interference and ensure that defect features are presented in a realistic and detailed manner.

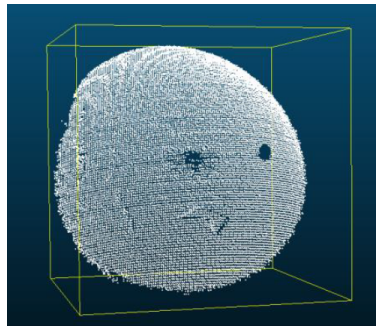

Fig. 3. 3D reconstruction point cloud of a ceramic ball.

There are numerous advanced point cloud processing models, such as PointNet [19], Point-Transformers [20], TEASER++ [21], *etc.* The first two create the point clouds, while the latter brings the recognised point clouds into alignment. Among these point cloud models, PointNet is a pioneer and robust deep learning network used for processing 3D point cloud data. Its core structure includes an input layer, a feature extraction layer, and a fully connected layer, which achieves robust processing of point cloud disorder through max pooling. Although PointTransformers and TEASER++ are the current performance leaders, PointNet possesses the obvious advantages of effectiveness, computer efficiency, and architectural simplicity for segmentation tasks. Therefore, we are herein about to utilise the PointNet model to process the point cloud of a ceramic ball reconstructed by a binocular structured light system. A detailed flowchart to illustrate the subsequent individual stages of data processing and analysis is shown in Fig. 4.

Metrol. Meas. Syst., Vol. 33 (2026), No. 1, pp. 1–16
DOI: 10.24425/mms.2026.158367

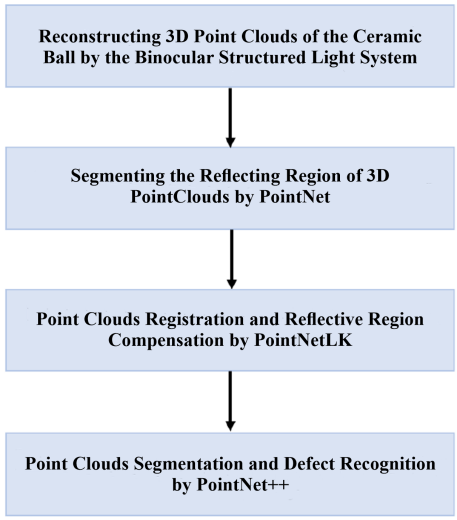

Fig. 4. Flow diagram of the point cloud processing and analysis.

3. Binocular Point Cloud Registration and Reflection Compensation in Ceramic Balls

3.1. PointNet and Reflective Region Segmentation

The PointNet network architecture is depicted in Fig. 5. It employs shared *Multilayer Perceptrons* (MLPs) to perform point-wise feature extraction, subsequently aggregating individual point features into a global descriptor via max pooling, thereby allowing effective representation of overall shape and structure [22]. To mitigate variations caused by rotation and translation, the network incorporates a T-Net submodule that aligns input point clouds, ensuring that the extracted features exhibit both rotation and translation invariance.

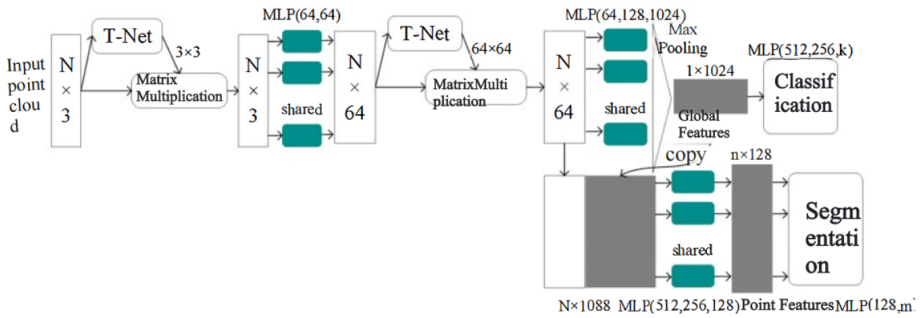

Fig. 5. PointNet network architecture.

Experiments were conducted using a self-constructed 3D reconstructed point cloud dataset of ceramic balls, encompassing both original samples and augmented samples subjected to random rigid transformations, resulting in a dataset consisting of 304 samples. The PointNet network architecture was used to segment the specular reflection regions within the point clouds, with the experimental results detailed in Table 1.

Table 1. Experimental results of reflective region segmentation for ceramic balls.

Evaluation Metrics	Reflection Region Segmentation	ShapeNet
Accuracy/%	93.60	83.70
mIoU/%	91.13	80.41

Experimental validation reveals that the model can achieve an accuracy rate of 93.60% and a mean Intersection over Union (mIoU) of 91.13% in segmenting specular reflection regions of the ceramic ball point clouds. As well known, ShapeNet is a widely used 3D point cloud dataset, commonly used as a sanity check. As a result, similar experiments on ShapeNet have shown that PointNet model performs robustly and has strong robustness in most segmentation tasks. The results shown in Table 1 fully demonstrate that the PointNet model used for point cloud segmentation of ceramic balls has an effective migration capability for our specific industrial scenario, *i.e.* highly reflective region segmentation.

These results demonstrate the high precision of the model in segmenting specular regions. This performance advantage primarily stems from the enhanced capacity of the network to capture features of surface curvature. To visually illustrate the effectiveness of segmentation, the results are visualised in Fig. 6, where the blue point cloud represents the predicted ceramic ball surface, and the red point cloud denotes the identified specular regions. In subsequent processing, removing the red point cloud enables the generation of a reflection-free point cloud dataset.

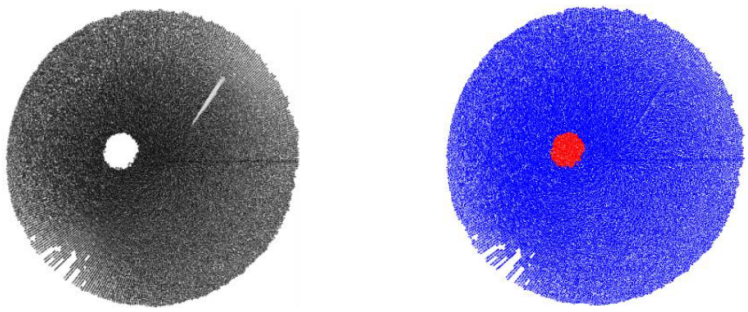

(a) (b)

Fig. 6. Reflection region segmentation in the point cloud of a ceramic ball: a) original point cloud, b) reflection region segmentation.

3.2. PointNetLK and Point Cloud Registration

PointNetLK is an innovative method for 3D point cloud registration that integrates deep learning with traditional optimisation frameworks [23, 24]. By combining the feature extraction capabilities of PointNet and the optimisation mechanisms of the *Lucas-Kanade* (LK) algorithm, it addresses the challenges inherent in point cloud alignment. The network architecture of PointNetLK is illustrated in Fig. 7.

Employing the *Inverse Compositional* (IC) formulation to refine the LK algorithm tackles its fundamental limitation, where the conventional LK necessitates recomputing the Jacobian matrix for the transformed source point cloud at every iteration. The crux of the IC approach resides in swapping the operational roles between the template and source point clouds: within

Metrol. Meas. Syst., Vol. 33 (2026), No. 1, pp. 1–16
DOI: 10.24425/mms.2026.158367

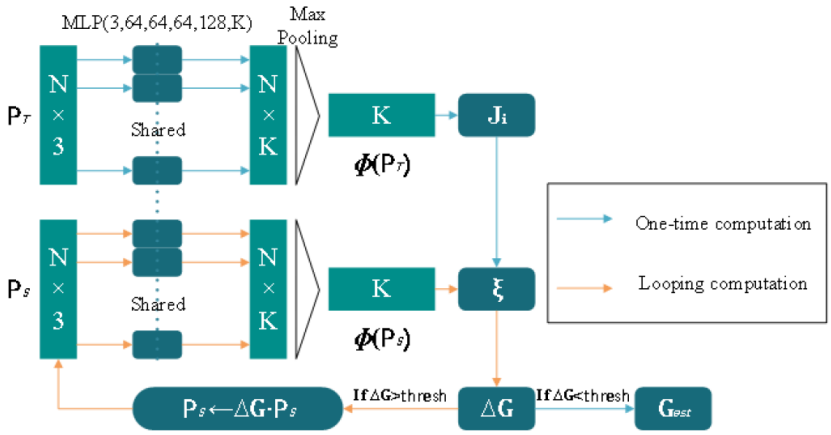

Fig. 7. PointNetLK network architecture.

each iterative step, an incremental transformation update is initially imposed on the template point cloud, subsequently applying the inverse of this incremental transformation to the source point cloud. This incurs defining the Jacobian matrix:

$$J = \frac{\partial \left[\phi \left(G^{-1} \cdot P_T\right)\right]}{\partial \xi}. \tag{1}$$

By implementing this approach, the Jacobian matrix is computed for the template point cloud rather than the source, and this computation is executed only once prior to optimisation initiation, eliminating the need for iterative updates. The Jacobian columns are approximated using finite-difference gradients within a stochastic gradient framework:

$$J_i = \frac{\phi \left(\exp\left(-t_i T_i\right) \cdot P_T\right) - \phi\left(P_T\right)}{t_i}, \tag{2}$$

where $t_i$represents the infinitesimal perturbations of the ξ twist parameters.The twist parameters can then be computed as ξ:

$$\xi = J^{+}\left[\phi\left(P_s\right) - \phi\left(P_T\right)\right], \tag{3}$$

where J^{+}denotes the J Moore–Penrose pseudoinverse of the Jacobian matrix. The entire iterative algorithm computes the twist parameters using the equation ξ to generate an ΔG incremental update for the source point cloud at each iteration P_s. When the ΔG incremental update falls below a predefined threshold, the iterative optimization is terminated. The final transformation estimate G_{est} is obtained by accumulating all incremental updates computed throughout the ΔG iteration loop:

$$G_{est} = \Delta G_n \cdot \ldots \cdot \Delta G_1 \cdot \Delta G_0. \tag{4}$$

During network training, the loss function is defined as the following Frobenius norm:

$$Loss = \left|\left|\left(G_{est}\right)^{-1} \cdot G_{gt} - I_4\right|\right|_F, \tag{5}$$

where G_{gt} as the true transformation matrix I_4 is the 4×4 identity matrix. This approach exhibits superior computational efficiency, as it eliminates the need for matrix logarithm operations during the training phase. Following the completion of specular region segmentation, the dual-viewpoint

point cloud data, with reflection components removed, is fed into the PointNetLK network for registration. To benchmark performance, a conventional *Coherent Point Drift* (CPD) + *Iterative Closest Point* (ICP) registration algorithm is employed for comparative analysis. In the domain of 3D point cloud registration, *Root Mean Square Error* (RMSE) serves as the principal evaluation metric.

$$RMSE = \sqrt{\frac{\sum_{i=1}^{n} \|s_i - t_i\|_2^2}{n}}, \tag{6}$$

where n is the number of corresponding point pairs between two different coarse registered point clouds obtained from the binocular structured light system, and s_i and t_i are the corresponding points that belong to the source and target point clouds respectively. A lower RMSE value indicates lower registration error and higher registration accuracy. The experimental results comparing the two registration methods are presented in Table 2.

Table 2. Comparison of two different point cloud registration algorithms.

Evaluation metric	**PointNetLK**	**CPD+ICP**
RMSE/mm	0.004730	0.1544

As demonstrated in the table above, PointNetLK based on deep learning exhibits groundbreaking advantages in the binocular point cloud registration task for ceramic balls. Its registration accuracy shows a significant improvement over the traditional method (CPD+ICP), with the RMSE reduced by two orders of magnitude, achieving micrometre-level precision. The comparative registration results are illustrated in Fig. 8. In Fig. 8a, the initial state of dual-viewpoint clouds is displayed,

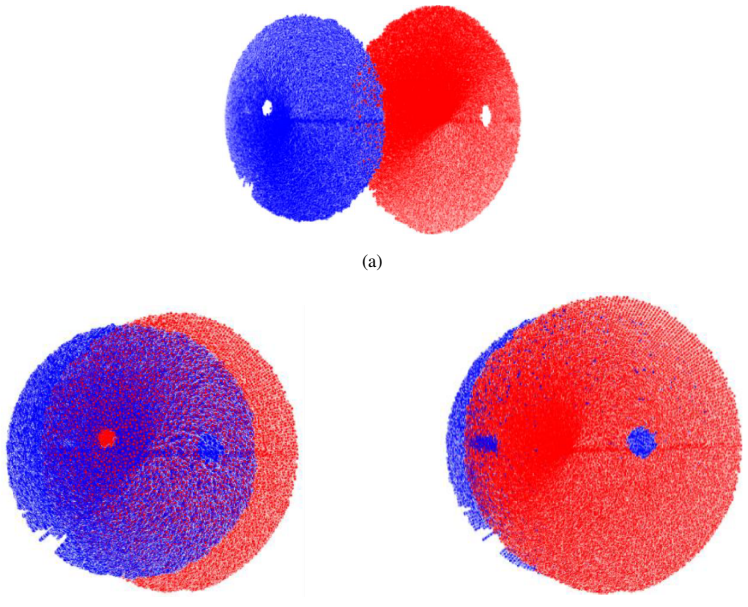

Fig. 8. Comparison of point cloud registration effects between PointNetLK and CPD+ICP: a) initial point clouds, b) PointNetLK registration effect and c) CPD+ICP registration effect.

where the blue points represent the target point cloud, and the red points denote the source point cloud. Figures 8b and 8c, respectively, show the registration outcomes of PointNetLK and CPD+ICP. Notably, after PointNetLK registration, the alignment between the source and target point clouds becomes markedly tighter.

4. Detection of Defects in Ceramic Balls with Binocular Point Cloud

4.1. PointNet++ Network

To address the limitations of PointNet in local feature modelling and density adaptability, PointNet++ implements multiple key improvements in both network architecture and training mechanisms [25, 26]. The enhanced network architecture for the PointNet++ segmentation task is illustrated in Fig. 9.

In Fig. 9, $N, N1, N2$ are the numbers of points in the point set, and $N > N1 > N2$, d is the coordinate dimensions of points, c denotes the dimensions of other point features, K indicates the size of grouped point sets, and k expresses the number of segmentation classes. First, PointNet++ employs a hierarchical "sampling–grouping–feature extraction" *set abstraction* (SA) framework, recursively delving into geometric information across diverse spatial scales within point clouds. Through progressive downsampling and localised encoding at successive layers, the model significantly enhances its sensitivity to microscopic details (such as edges and textures) while preserving information on the global shape, thereby providing richer and more stable multi-scale feature representations. Second, PointNet++ introduces a *Multi-Scale Grouping* (MSG) strategy within each set abstraction module. By parallelising neighbourhoods with various radii, it simultaneously captures both large-scale contextual features and fine-grained local details.

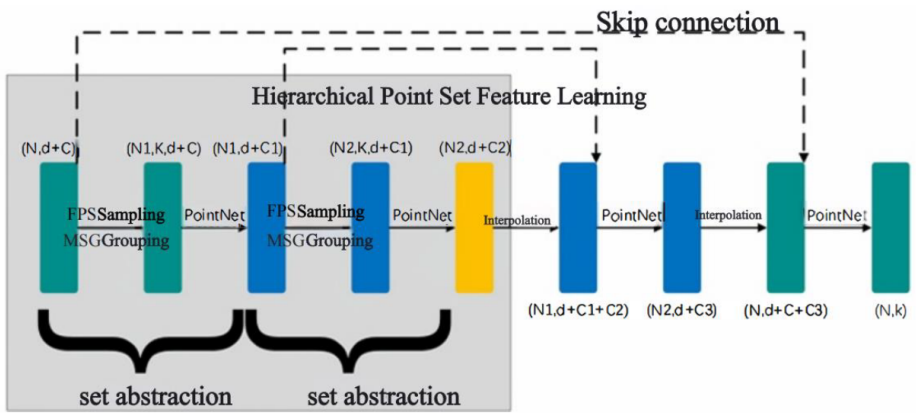

Fig. 9. Network architecture of PointNet++ for segmentation task.

After multiple optimisations are performed, the PointNet++ network generates a set of score weights corresponding to each segmentation class for each point. Finally, by comparing these weights and selecting the maximum value, the category assignment can be accurately determined for each point. This workflow demonstrates greater stability and precision when processing point cloud segmentation scenarios characterised by significant density variations and complex geometric structures.

4.2. Defect Segmentation Experiment

The experiment is based on the PyTorch deep learning framework and uses an RTX 4060 graphics card for model training. The specific configuration of the experimental environment is detailed in Table 3.

Table 3. Experimental environment.

Environment Name	
Operating System	Ubuntu 22.04.5
GPU	RTX4060
CPU	13th Gen Intel(R) Core(TM) i9-13900HX 2.20 GHz
RAM	32.0 GB
Deep Learning Framework	PyTorch (2.1.1)
Interpreter	Python (3.11)
Compute Unified Device Architecture Version	CUDA (12.1)

A total of 404 point clouds from ceramic balls were collected in this experiment, encompassing two defect types: pits and scratches. The raw point clouds initially underwent butterfly subdivision upsampling. Subsequently, the processed data were fed into the PointNetLK network to eliminate reflection regions while completing viewpoint registration and compensation. Following this pipeline, 202 valid samples were retained, comprising 105 pit-defected ceramic ball point clouds and 97 scratch-defected counterparts, all manually annotated for defects. Finally, the dataset was divided according to a 7:2:1 ratio into training, testing, and validation sets. The details of the distribution of the ceramic ball samples are summarised in Table 4.

Table 4. Sample division results for silicon nitride ceramic balls.

Defect Type	**Number of Points**	**Proportion**	**Label**
Pit	79275	0.5%	0
Scratch	44814	0.8%	1
Spherical Surface	18055911	98.7%	2

During the training of PointNet++, we used a batch size of 16 and selected the Adam optimizer with an initial learning rate set to 0.001. The learning rate was adjusted using a decay rate of 0.0001, triggering a reduction every 20 epochs. The input point clouds were sampled to 2048 points, and the entire training process spanned 250 epochs to ensure comprehensive learning of complex spatial features. The evolution of mIoU metrics across defect categories, spherical surfaces, and their average values throughout the epochs is illustrated in Fig. 10. The optimal performance results of the PointNet++ model are presented in Table 5.

Table 5. Optimal performance of PointNet++ for the segmentation task.

Evaluation Metric	**Scratch**	**Pit**	**Spherical Surface**	**Average**
mIoU	0.8113	0.8755	0.9070	0.8565
F1	0.8275	0.8848	0.9142	0.8663

Metrol. Meas. Syst., Vol. 33 (2026), No. 1, pp. 1–16
DOI: 10.24425/mms.2026.158367

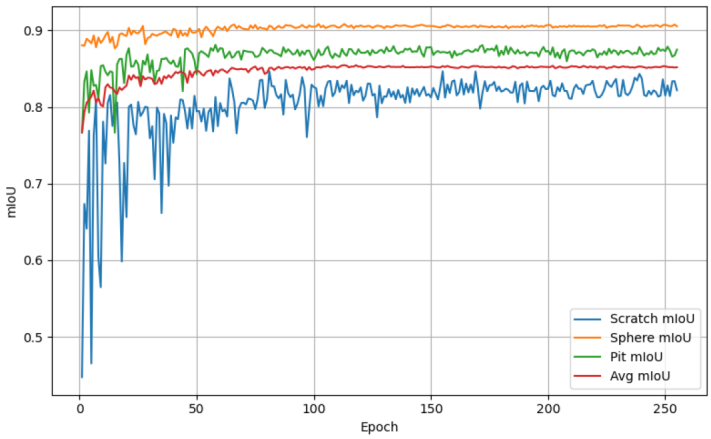

Fig. 10. Visualisation analysis of the experimental data for defect segmentation.

From the curves in Fig. 10, it is evident that during the initial training phase, the mIoU values for all categories exhibited significant fluctuations. As the number of iterations increased, these metrics rapidly rose and stabilised after approximately 100 epochs: The regular, well-sampled spherical surfaces (orange) converged first, with mIoU increasing from 0.8805 to 0.9070; followed by medium-sized pits (green), which ultimately stabilised at 0.8755; while linear, thin-boundary scratches (blue) started lowest (0.45) but surged quickly within the first 30 epochs to reach 0.80, maintaining slight oscillations thereafter. The overall average mIoU (red) improved consistently from 0.7667 to 0.8565, demonstrating that the model achieved a balanced and efficient segmentation capability for both types of defects.

Figure 11 and Fig. 12, respectively, illustrate the visual detection and recognition results of the improved PointNet++ network corresponding to two pit defects and scratch defects for silicon nitride ceramic balls. In Figs. 11 and 12, red, green, and blue point clouds are used to mark pit

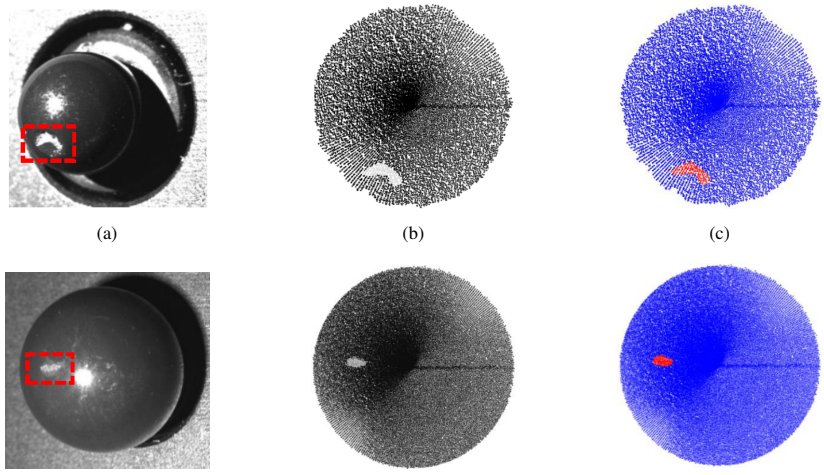

Fig. 11. Results for detection of pit defects in a ceramic ball.

defects, scratch defects, and normal reflection surface regions, respectively, forming an intuitive spatial distribution map of defects. The experiments validate the feasibility and effectiveness of the improved PointNet++ network in detecting various surface defects on silicon nitride ceramic balls.

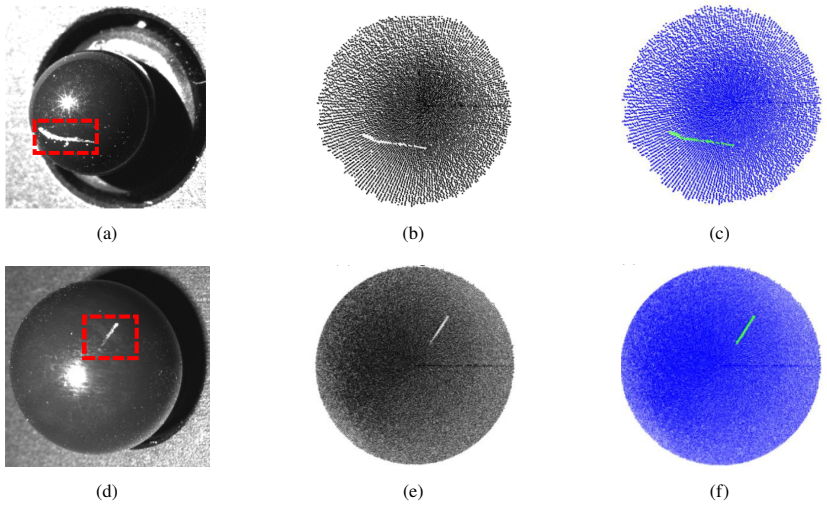

Fig. 12. Results for detection of scratch defects in a ceramic ball.

4.3. Analysis of the Ablation Study

An ablation study was conducted on two critical improvements of the PointNet++ model, SA and MSG, to evaluate their performance enhancement in silicon nitride ceramic ball surface defect segmentation tasks. The SA module enables hierarchical sampling and localised feature extraction, allowing the model to effectively capture local geometric structures within point clouds. Compared to the original PointNet model, incorporation of the SA module resulted in a significant improvement in the mIoU metric for segmentation tasks, demonstrating the crucial role of local features in identifying surface defects. Furthermore, optimising *Single-Scale Grouping* (SSG) to the MSG strategy involved employing multiple search radii around each sampled point to extract multi-scale local features. This approach improved the robustness of the model to defects of varying sizes and shapes. The experimental results showed that the combination of the MSG strategy led to further improvements in the mIoU metric. The experimental results are presented in Table 6.

Table 6. Results of the ablation study.

Model	**+SA**	**+MSG**	**Avg mIoU**	**F1**
PointNet			0.7887	0.8020
PointNet++(SSG)	✓		0.8303	0.8438
PointNet++(MSG)	✓	✓	0.8565	0.8663

Experiments demonstrate that the hierarchical feature learning and MSG strategy based on the improved PointNet++ significantly enhance the segmentation accuracy and robustness to detect small defects, such as pits and scratches, on the surface of silicon nitride ceramic balls, exhibiting distinct advantages over the traditional PointNet method.

In summary, both PointNetLK and PointNet++ we used essentially utilise depth features as state feedback to actively estimate and compensate for the uncertainty of point cloud loss and noise caused by reflection and occlusion through iterative optimisation (feature rollback). This data-driven compensation mechanism is similar to the model reference adaptive control strategy of control theory in the core logic of estimation compensation.

The main novelty lies in innovatively transferring and implementing this idea from the traditional field of dynamic system control to static point cloud data processing for visual tasks. We did not explicitly model system dynamics but implicitly learned how to achieve robust alignment in the feature space through deep networks to compensate for uncertainty at the data level. This provides a new approach to dealing with uncertainty issues in complex visual perception that echoes control theory but has a different implementation path.

5. Conclusions

This paper addresses the challenge of high reflection interference encountered when applying binocular structured light for detection of surface defects on silicon nitride ceramic balls. It proposes a novel solution integrating a PointNetLK point cloud registration network with an improved PointNet++ point cloud segmentation network, enabling high-precision and non-destructive testing of typical defects such as pits and scratches on surfaces of ceramic ball.

The proposed method achieved an accuracy rate of 93.6% on a self-developed ceramic ball point cloud dataset, effectively localising and eliminating highly reflective regions. PointNetLK accomplished micrometeor level registration accuracy (RMSE = 0.0047mm), demonstrating a two-order-of-magnitude enhancement compared to the traditional CPD+ICP method and significantly optimizing reflection compensation. By incorporating a MSG strategy, PointNet++ achieved an average mIoU of 0.8565 for pit segmentation (mIoU = 0.8755) and scratch segmentation (mIoU = 0.8113), with ablation studies confirming significant contributions from both the SA and MSG modules, yielding an 8.78% improvement over conventional PointNet.

This method provides a new paradigm for detecting surface defects on highly reflective ceramic balls, and its robustness and accuracy are sufficient to meet the requirements of industrial batch testing. Future work will focus on deep integration with adaptive robot systems to achieve closed-loop detection decision operations, which is of great significance to improve the automation and intelligence level of the detection of surface defects in ceramic ball.

Acknowledgements

This work was supported by the Jiangsu Province Industry-University-Research Collaboration Project (No. BY20240504), and the Lianyungang Major Technology Research Project of Open Bidding to Select the Best Candidates (No. CGJBGS2202).

References

[1] Wang, P., Li, S., Wu, Y., & Zhao, J. (2024). Initiation of secondary surface crack in the ring raceway of silicon nitride full ceramic bearing. *Journal of Ceramic Processing Research*, *25*(4), 694–703. https://doi.org/10.36410/jcpr.2024.25.4.694

[2] Boschetto, F., Rondinella, A., & Marin, E. (2024). Biological Activity of Silicon Nitride Ceramics: A Critical Review. *Materials*, *17*(22), 5548. https://doi.org/10.3390/ma17225548

[3] Gu, G., Wang, H., Miao, X., Yan, J., & Du, J. (2025). Non-destructive detection of ceramic ball surface defects based on improved YOLOv8. *Metrology and Measurement Systems*, 1. https://doi.org/10.24425/mms.2025.152777

[4] Baraheni, M., & Amini, S. (2019). Predicting subsurface damage in silicon nitdata1; revised data2; accepted data3; available online data4ride ceramics subjected to rotary ultrasonic assisted face grinding. *Ceramics International*, *45*(8), 10086–10096. https://doi.org/10.1016/j.ceramint.2019.02.055

[5] Malyshev, A. V., Vlasov, V. A., Petrova, A. B., & Surzhikov, A. P. (2019). Effect of ball milling on defects level, Curie point and microstructure of LiTiZn ferrite ceramics. *Journal of Thermal Analysis and Calorimetry*, *138*(3), 2197–2203. https://doi.org/10.1007/s10973-019-08823-3

[6] Zhao, Z. (2020). Review of non-destructive testing methods for defect detection of ceramics. *Ceramics International*, *47*(4), 4389–4397. https://doi.org/10.1016/j.ceramint.2020.10.065

[7] Deneuville, F., Duquennoy, M., Ouaftouh, Ourak, M., Jenot, F., & Desvaux, S. (2008). High frequency ultrasonic detection of C-crack defects in silicon nitride bearing balls. *Ultrasonics*, *49*(1), 89–93. https://doi.org/10.1016/j.ultras.2008.06.010

[8] Chlebus, E., Kuźnicka, B., Dziedzic, R., & Kurzynowski, T. (2014). Titanium alloyed with rhenium by selective laser melting. *Materials Science and Engineering A*, *620*, 155–163. https://doi.org/10.1016/j.msea.2014.10.021

[9] Lei, Z., Sun, J., Zhu, X., Ma, H., & Liang, L. (2022). Error-compensated one-dimensional convolutional neural network-based ultrasonic defect signal recognition method for flat ceramic membranes. *Ceramics International*, *49*(3), 5391–5400. https://doi.org/10.1016/j.ceramint.2022.10.062

[10] Zhang, K., Fu, L., Wang, Z., Sun, Y., & Liu, C. (2017). Research on surface defect detection of ceramic ball based on fringe reflection. *Optical Engineering*, *56*(10), 1. https://doi.org/10.1117/1.oe.56.10.104104

[11] Liao, D., Cui, Z., Zhu, Z., Jiang, Z., Zheng, Q., & Wu, N. (2023). A nondestructive recognition and classification method for detecting surface defects of Si_3N_4 bearing balls based on an optimized convolutional neural network. *Optical Materials*, *136*, 113401. https://doi.org/10.1016/j.optmat.2022.113401

[12] Xu, G., Liu, C., Hu, D., Xiong, Y., Gu, P., & Liu, X. (2025). Enhanced real-time defect detection for ceramic bearing balls using advanced feature extraction and optimization. *Measurement Science and Technology*, *36*(5), 055014. https://doi.org/10.1088/1361-6501/add045

[13] Li, X., Chen, L., Liu, S., Shao, M., Hu, R., Li, R., Li, Y., & An, D. (2024). A method for multi-view surface defect detection of Si_3N_4 ceramic bearing balls integrating features enhanced by the Gabor salient domain. *Measurement Science and Technology*, *35*(8), 085205. https://doi.org/10.1088/1361-6501/ad4812

[14] Jiang, Y., Hu, K., Zhang, X., Zheng, Q., Li, J., & Wu, N. (2023). A coupling enhancement algorithm for ZrO_2 ceramic bearing ball surface defect detection based on cartoon-texture decomposition model and multi-scale filtering method. *Optics Communications*, *554*, 130214. https://doi.org/10.1016/j.optcom.2023.130214

[15] Yu, D., Zhang, H., Zhang, X., Liao, D., & Wu, N. (2021). SI_3N_4 ceramic ball surface defects' detection based on SWT and nonlinear enhancement. *Mathematical Problems in Engineering*, *2021*, 1–9. https://doi.org/10.1155/2021/4922315

[16] Ma, J., Meng, X., Wang, H., Jiang, F., Wang, S., & Kodagoda, S. (2024). Comprehensive improvement of binocular structured light calibration method based on radical-conservative cooperative particle swarm. *Sensors*, *24*(24), 8155. https://doi.org/10.3390/s24248155

[17] Pistellato, M., Bergamasco, F., Albarelli, A., Cosmo, L., Gasparetto, A., & Torsello, A. (2019). Robust phase unwrapping by probabilistic consensus. *Optics and Lasers in Engineering*, *121*, 428–440. https://doi.org/10.1016/j.optlaseng.2019.05.006

[18] Heng, S., Li, G., Huang, H., Chang, Q., Zhang, Z., & Wang, Y. (2025). 3D reconstruction of a strongly reflective surface based on binocular line-structured light. *Applied Optics*, *64*(9), 2315. https://doi.org/10.1364/ao.553374

[19] Qi, C. R., Su, H., Mo, K., & Guibas, L. J. (2016). PointNet: Deep learning on point sets for 3D classification and segmentation. *arXiv (Cornell University)*. https://doi.org/10.48550/arxiv.1612.00593

[20] Tang, Y., Wang, B., He, W., Qian, F., & Liu, Z. (2022). PointTransformer: Encoding human local features for small target detection. *Computational Intelligence and Neuroscience*, *2022*, 1–10. https://doi.org/10.1155/2022/9640673

[21] Yang, H., Shi, J., & Carlone, L. (2020). TEASER: Fast and certifiable Point Cloud registration. *IEEE Transactions on Robotics*, *37*(2), 314–333. https://doi.org/10.1109/tro.2020.3033695

[22] Haznedar, B., Bayraktar, R., Ozturk, A. E., & Arayici, Y. (2023). Implementing PointNet for point cloud segmentation in the heritage context. *Heritage Science*, *11*(1). https://doi.org/10.1186/s40494-022-00844-w

[23] Aoki, Y., Goforth, H., Srivatsan, R. A., & Lucey, S. (2019). PointNetLK: Robust & Efficient Point Cloud Registration using PointNet. *arXiv (Cornell University)*. https://doi.org/10.48550/arxiv.1903.05711

[24] Kurobe, A., Sekikawa, Y., Ishikawa, K., & Saito, H. (2020). CORSNET: 3D Point Cloud registration by deep neural Network. *IEEE Robotics and Automation Letters*, *5*(3), 3960–3966. https://doi.org/10.1109/lra.2020.2970946

[25] Qi, C. R., Yi, L., Su, H., & Guibas, L. J. (2017). PointNet++: deep hierarchical feature learning on point sets in a metric space. *arXiv (Cornell University)*. https://doi.org/10.48550/arxiv.1706.02413

[26] Sorokin, M. I., Zhdanov, D. D., & Zhdanov, A. D. (2024). Conversion of Point Cloud data to 3D models using PointNet++ and Transformer. *Programming and Computer Software*, *50*(3), 249–256. https://doi.org/10.1134/s0361768824700051

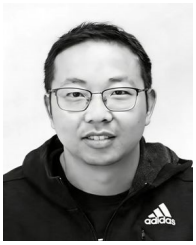

Gang Cheng received his M.Sc. degree from Jiangsu University, China, in 2013. He is currently a laboratory engineer at the School of Mechanical Engineering, Yancheng Institute of Technology. His research interests primarily lie in precision manufacturing and quality inspection.

Xuyi Miao received his B.Sc. degree from Yancheng Institute of Technology, China, in 2022. He is a full-time graduate student in Yancheng Institute of Technology, majoring in system and automatic control, mainly focusing on defect detection.

Guoqing Gu received his Ph.D. degree from Nanjing University of Aeronautics & Astronautics, China, in 2013. He is currently an Associate Professor of the School of Civil Engineering of Yancheng Institute of Technology. His research activity focuses on experimental mechanics.

Jianzhou Du received his Ph.D. degree from Nanjing University of Aeronautics and Astronautics, China, in 2014. He is currently an Associate Professor of the School of Materials Science and Engineering, Yancheng Institute of Technology. His research focuses on advanced ceramics and structures.

Jingyi Yan received his M.Sc. degree in mechanical engineering from Carnegie Mellon University, USA, in 2013. His research focuses on the structural development and applications of high-performance alumina, silicon nitride, and zirconia ceramics.